Sensors and Actuators B 262 (2018) 625–636

Contents lists available at ScienceDirect

Sensors and Actuators B: Chemical

journal homepage: www.elsevier.com/locate/snb

# Fabrication of whole-thermoplastic normally closed microvalve, micro check valve, and micropump

Adel Pourmand[a,b,c,1], Seyed Ali Mousavi Shaegh[a,b,d,e,1], Habib Badri Ghavifekr[c,***], Esmaiel Najafi Aghdam[c], Mehmet Remzi Dokmeci[a,b,f,g,h], Ali Khademhosseini[a,b,f,g,h,i,j,k,l,m,**], Yu Shrike Zhang[a,b,f,*]

[a] Division of Engineering in Medicine, Department of Medicine, Brigham and Women's Hospital, Harvard Medical School, Cambridge, MA, 02139, USA
[b] Harvard-MIT Division of Health Sciences and Technology, Massachusetts Institute of Technology, Cambridge, MA, 02139, USA
[c] Department of Electrical Engineering, Sahand University of Technology, Tabriz, 5331711111, Iran
[d] Orthopedic Research Center, Mashhad University of Medical Sciences, Mashhad, 9176699199, Iran
[e] Clinical Research Unit, School of Medicine, Mashhad University of Medical Sciences, Mashhad 9176699199, Iran
[f] Wyss Institute for Biologically Inspired Engineering, Harvard University, Boston, MA, 02115, USA
[g] Center for Minimally Invasive Therapeutics (C-MIT), University of California-Los Angeles, Los Angeles, CA, 90095, USA
[h] Department of Radiology, David Geffen School of Medicine, University of California-Los Angeles, Los Angeles, CA, 90095, USA
[i] Department of Bioengineering, Department of Chemical and Biomolecular Engineering, Henry Samueli School of Engineering and Applied Sciences, University of California-Los Angeles, Los Angeles, CA, 90095, USA
[j] California NanoSystems Institute (CNSI), University of California-Los Angeles, Los Angeles, CA, 90095, USA
[k] WPI-Advanced Institute for Materials Research, Tohoku University, Sendai, 980-8577, Japan
[l] Nanotechnology Center, King Abdulaziz University, Jeddah, 21569, Saudi Arabia
[m] College of Animal Bioscience and Technology, Department of Bioindustrial Technologies, Konkuk University, Hwayang-dong, Kwangjin-gu, Seoul, 143-701, Republic of Korea

ARTICLE INFO

*Article history:*
Received 28 August 2017
Received in revised form
27 November 2017
Accepted 20 December 2017
Available online 28 December 2017

*Keywords:*
Thermoplastic materials
Thermoplastic polyurethane
Microfluidic valves and pumps
Laser micromachining
Thermal bonding

ABSTRACT

There is a critical need to develop fabrication methods for rapid and cost-effective prototyping of thermoplastics-based microfluidics in academic research laboratories. This paper presents a method for the fabrication of whole-thermoplastic microfluidic functional elements, including a pneumatic (gas-actuated) normally closed microvalve, a micro-check valve, and a pneumatic dual-phase micropump. All devices were made from thermoplastic polyurethane (TPU) and poly(methyl methacrylate) (PMMA). The fabrication process consisted of only laser micromachining and thermal fusion bonding without need to perform any particular chemical treatment or use a master mold. These features enable the widespread adaptation of this method in academic research settings. Characterizations revealed that the fabricated normally closed microvalve could stop liquid flows at pressures lower than 2 psi in its passive operation mode where no pressure was used for valve actuation. The check valve could block liquid flows with liquid pressures of up to 30 psi in its reverse mode of operation while it could allow liquid to pass through in its forward mode. In addition, the micropump, which consisted of two check valves and a pneumatic uni-diaphragm displacement chamber, could pump liquid at an average flow rate of $87.6 \pm 5.0$ μL/min using an actuation frequency and pressure of 1 Hz and ±5 psi, respectively. Taken together, the developed low-cost whole-thermoplastic microfluidic functional elements could be employed for the fabrication of various lab-on-a-chip applications.



* Corresponding author at: Division of Engineering in Medicine, Department of Medicine, Brigham and Women's Hospital, Harvard Medical School, Cambridge, MA, 02139, USA.
** Corresponding author at: Center for Minimally Invasive Therapeutics (C-MIT), University of California-Los Angeles, Los Angeles, CA, 90095, USA.
*** Corresponding author at: Department of Electrical Engineering, Sahand University of Technology, Tabriz, 5331711111, Iran.
*E-mail addresses:* badri@sut.ac.ir (H.B. Ghavifekr), khademh@ucla.edu (A. Khademhosseini), yszhang@research.bwh.harvard.edu (Y.S. Zhang).
[1] Equal contribution as first author.

https://doi.org/10.1016/j.snb.2017.12.132
0925-4005/

## 1. Introduction

Recently, there has been an interest in the microfluidics community to further develop thermoplastics-based devices for chemical and biological applications [1–4]. This need mostly stems from issues related to polydimethylsiloxane (PDMS) such as vapor permeability [5–7], absorbance of small molecules [8,9], leaching of uncrosslinked oligomers [8,10], and incompatibility with large-scale manufacturing [1,2,4,11]. To this end, it is of great importance to innovate fabrication methods that allow for the production of various microfluidic functions using thermoplastics in a cost-effective and rapid fashion. Importantly, supporting academic labs and small companies with such fabrication methods can accelerate transition of basic microfluidic discoveries into commercialization segment where thermoplastics-based microfabrication technologies are being employed to manufacture low-cost consumables [3,11]. Thermoplastics are optically transparent [12,13], and possess good chemical compatibility [14] and appropriate biocompatible properties [1–3]. They can be employed for mass production of microfluidic chips using commercially available methods including microinjection molding and hot embossing [12,15–17].

Thus far, thermoplastic materials have been employed for fabrication of microfluidic systems to realize various functions including microcytometry [18], methanol detection [18], droplet generation [19], micromixing [20,21], electrophoresis [22], liquid chromatography [23], microbioreactors [24], as well as centrifugal microfluidics and lab-on-a-disk platforms [25–29]. Although the inherent properties of thermoplastics provide high robustness to physical deformation and resistance to different substances, the widespread use of these materials has been limited due to the challenging implementation of microfluidic actuators such as microvalves and micropumps in thermoplastic chips [2]. Three-dimensional (3D) printing is an emerging technology for the fabrication of robust microfluidics potentially with implemented microactuators in hard resins [30–33]. However, at this stage the use of this method is still limited in the types of materials, cost, and printing resolution [30,33,34].

The most common method of implementing microvalves in hard plastic chips is mainly based on the integration of a thin PDMS film, as an elastic membrane, within various rigid substrates including poly(methyl methacrylate) (PMMA) [35], cyclic olefin co-polymer (COC) [36–38], fluoropolymers [39], polyvinyl chloride (PVC) [40], polyethylene [41], or other thermoplastic materials [42]. This process requires additional steps during chip fabrication due to the challenges of bonding PDMS membrane to thermoplastics, besides the remaining concerns of the negative properties associated with the PDMS film for cell studies, drug screening, point-of-care diagnosis, and organ-on-a-chip applications [2,4].

There have been several efforts in the use of thermoplastic elastomers as a substitute of PDMS to implement whole-thermoplastic microvalves. Available literature includes polystyrene [43], Viton® [44], Teflon [39,45,46], photocurable liquid-based perfluoropolyethers [47,48], resin-based polyurethane membrane [49], as well as styrene-ethylene/butylene-styrene (SEBS) block copolymers [50]. Thermoplastic polyurethane (TPU) is another thermoplastic elastomer that is compatible with organic solvents [51,52] and suitable for rapid prototyping [53,54]. TPU is an important category of thermoplastic elastomer with widespread use in biomedical applications due to its strong biocompatibility and proper thermo-mechanical properties [54,55].

Recently, we have developed a rapid prototyping method to fabricate whole-thermoplastic multi-layer normally open pneumatic membrane microvalves (push-seal Quake valve) and peristaltic micropumps using laser-micromachined TPU and PMMA components [54]. In the current paper, the rapid prototyping method was further modified to produce built-in normally closed whole-thermoplastic microvalves using PMMA sheets as the substrates and TPU film as the elastomeric membrane. $CO_2$ laser machining was employed to cut PMMA and TPU sheets while thermal fusion bonding assisted the attachment of the layers without any particular chemical (solvent) treatment. This fabrication method was also used to fabricate whole-thermoplastic built-in membrane-based micro-check valves. In additional, a design of a dual-phase micropump, made of two membrane-based micro-check valves and a pneumatic uni-diaphragm displacement chamber, was successfully developed for the first time. The fabricated microfluidic actuators revealed high performance for various microfluidic tasks including flow control, valving, and liquid pumping. The actuators can be easily fabricated and implemented within thermoplastic microfluidic chips for applications where integrated on-chip functions are desired. This fabrication technology may also be used to transfer conventional point-of-care and organ-on-a-chip platforms from PDMS-based materials [2,4,56] to whole-thermoplastic devices.

## 2. Experimental

### 2.1. Materials and apparatus

PMMA sheets with a thickness of 2 mm (McMaster, USA) were used to make thick layers during chip fabrication. PMMA films with a thickness of 125 μm (Goodfellow, USA) were utilized for the fabrication of microchannels. TPU films with a thickness of 25 μm (PT9200US NAT 1.0 mil, Covestro LLC, USA) were used to fabricate flexible membranes employed in the architecture of the microvalve, micro-check valve, and the micropump (Fig. 1).

A $CO_2$ laser machine (VLS 2.30, Universal Laser Systems, USA) with a wavelength of 10.6 μm and a maximum power of 25 W was employed to engrave and cut PMMA substrates and TPU films. Required thermal treatment and thermal bonding processes were performed in a vacuum oven (Isotemp vacuum oven 280A, Fisher Scientific, USA). Compressed nitrogen gas was used to drive liquid flow into microfluidic chips with the implemented microvalve and micro-check valve. Vacuum, from the laboratory central vacuum line, along with the compressed nitrogen gas, were used to actuate microvalve and micropump (Fig. 2). Tygon® tubing (Cole-Parmer, USA) with an inner diameter of 508 μm was utilized to connect chips to the reservoirs and controllers.

### 2.2. Design of the microvalve

The design of the normally closed valve is shown in Fig. 3a–c. The microvalve consisted of a liquid chamber with an obstacle embedded in the 125-μm PMMA layer with a width of 400 μm, a TPU membrane, and a control chamber for membrane actuation. All layers (including TPU membrane, PMMA film, and both PMMA substrates) were bonded together using a single-step thermal fusion bonding process. The obstacle was also bonded to the TPU during the process but its bonding strength was very weak due to the presence of the marker ink and could be easily detached during liquid loading at the first run. When liquid flow is required, the microvalve is activated by applying vacuum to the control chamber, which is located above the TPU membrane. The upward displacement of the membrane allows the liquid to flow through the valve. In this valve design, the necessity of having round channels in the architecture of the valve, which is common for normally open valves, such as the Quake valve [57], is eliminated. Thus, the fabrication process is more straightforward requiring fewer steps. The architecture of the valve was also employed to fabricate a micro-check valve and a micropump, as discussed in the next sections.

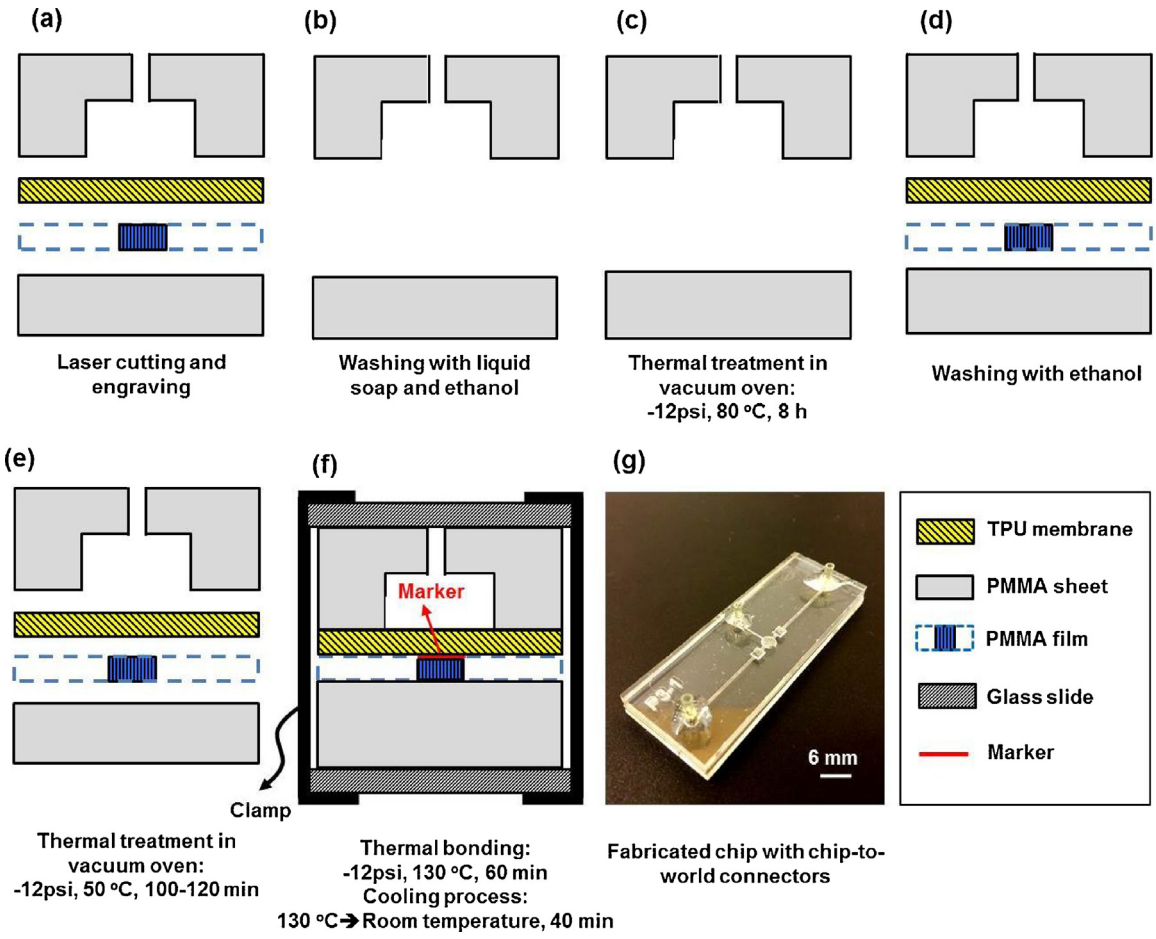


**Fig. 1.** Schematic illustrations of the fabrication process. (a) Laser cutting and engraving of PMMA specimens and TPU membrane; (b) washing with liquid detergent and pure ethanol; (c) thermal treatment of PMMA substrates;(d) washing with pure ethanol; (e) thermal treatment of all layers including membrane in vacuum oven; (f) marked using marker, alignment, thermal bonding, and cooling down processes. (g) Photograph showing a fabricated chip with embedded micropump.

### 2.3. Fabrication process

A multi-layer fabrication method was developed to create various microfluidic functional elements including a normally closed microvalve, a micro-check valve, and a micropump. Different layers of the functional elements, in desired dimensions, were designed in the CorelDraw software and then sent to the laser machine for cutting and engraving (Fig. 1a). Laser-micromachined PMMA substrates were washed using a mixture of liquid soap and water (at volume ratio of 1:10) followed by rinsing using water and air-dry. Then PMMA substrates were gently cleaned using a paper towel impregnated in pure ethanol (Fig. 1b). Afterwards, the PMMA substrates were thermally treated in a vacuum oven at a temperature of 80 °C and a vacuum pressure of −12 psi for at least 8 h to remove dissolved gases and ethanol entrapped within the bulk of PMMA (Fig. 1c). Subsequently, all PMMA sheets and TPU films were cleaned using a paper towel soaked with pure ethanol (Fig. 1d). After that, all cleaned sheets including PMMA film, PMMA substrates, and TPU film were kept in the vacuum oven at 50 °C and a pressure of −12 psi for 100–120 min (Fig. 1e). Again, this step enabled removal of dissolved gases and chemicals entrapped within the surface of all PMMA specimens and bulk of TPU membrane. This step is critical to obtain bubble-free bonding of different polymeric layers. Obstacles (ridges) in the middle of the microchannel located underneath the control chamber of the micro-check valve and the microvalve were carefully painted using a marker pen. It prevents irreversible adhesion and bonding of the obstacles to its adjacent TPU membrane during the thermal bonding process. It should be noted that, marker imprint can be conveniently removed through introducing a diluted solvent (e.g. 50% methanol) to the device post-fabrication. Thermoplastic substrates were aligned on top of each other and then sandwiched between two standard-sized glass slides using two binder clips with a width of 25 mm. The assembled chips were bonded using a thermal fusion bonding process at a temperature of 130 °C and a vacuum pressure of −12 psi for 1 h and then they were cooled down gradually from 130 °C to room temperature in 40 min (Fig. 1f). To obtain chip-to-world connectors for the fabricated microfluidic functional elements, appropriate plastic pipette tips were cut and fixed at the liquid ports and the actuation ports using commercially available fast-drying epoxy glue (Fig. 1g).

### 2.4. Experimental setup

A custom-made valve controller system was used to control and characterize the fabricated microfluidic components. The system consisted of solenoid valves (MH1, FESTO, USA), which were controlled by a programmable WAGO controller. A software interface was written in MATLAB for online communication with the WAGO controller to control the actuation of microvalves and micropumps. Vacuum line and nitrogen gas tank were connected to the solenoid valves, where their outlets were connected to the fabricated chips containing functional elements using Tygon® tubing (Fig. 2). Regulators with unit of psi were used to control the gas/vacuum pressure on the chips. Details of the controller system can be found in [56,58,59].

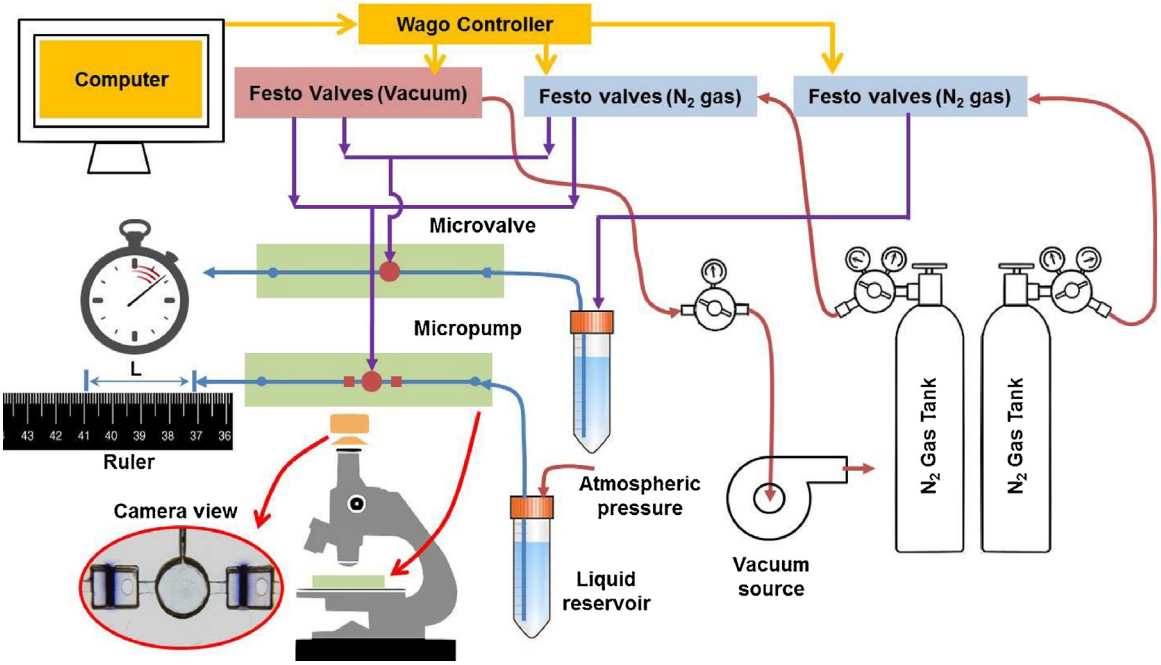


**Fig. 2.** Schematic of experiment setup to evaluate the fabricated functional elements.

## 3. Results and discussions

### 3.1. Characterizations of the normally closed microvalve

Figs. 3a and b show the operation of the normally closed microvalve. The valve is closed when no pressure is applied to the control chamber located above the membrane; it is open when negative pressure (relative to environment pressure) is applied to the control chamber. The normally closed valve had a four-layer symmetric architecture, shown in Fig. 3c. The fabricated valves, shown in Fig. 3d, were tested at various actuation pressures to characterize their behavior versus different pressures of liquid flow. Before tests, water containing food dye (50:1 vol ratio) was injected manually into the channel with implemented microvalve to ensure that no thermal bonding between the TPU membrane and the PMMA obstacle had occurred. Then, for valve characterizations, water containing food dye was injected into the channel with implemented microvalve using compressed nitrogen gas. To investigate the characteristics of the microvalve, various gas actuation pressures at +5, +3 psi, 0 psi (atmospheric pressure), −1.3 psi, −2.5 psi, or −3.5 psi, were applied to the actuation chamber, while liquid was injected to the channel in a pressure range of 0 psi to 3 psi, as shown in Fig. 3e and f.

At actuation pressure of +5 psi, the valve was completely closed for all liquid pressures. At actuation pressure of +3 psi, there was a leakage rate of $0.5 \pm 0.1$ μL/min when liquid pressure was set to 3 psi (Fig. 3e). Importantly, it was shown that the normally closed valve could provide leakage-free operations without any actuation pressure (i.e. passive mode) for liquid pressures of up to 2 psi; however, leakage rates of $4 \pm 0.3$ μL/min and $7 \pm 0.4$ μL/min were observed once the liquid pressure was elevated to 2.5 psi and 3 psi, respectively. During the passive mode of valve operation, no pressure was applied to the control chamber to keep it closed and the spring property of the membrane was the only resistance against the liquid flow. In addition, when the actuation pressure was set on vacuum values, the microvalve was open to allow for high liquid flow rates. At actuation pressure of −3.5 psi, the microvalve was completely open and liquid flow rate increased linearly with respect to inlet pressure (Fig. 3f). Since this valve has two states of open and closed, which is equal to an on/off switch, one can actuate it using +5 psi to close and −3.5 psi to open the valve at a liquid pressure of 3 psi.

Ren et al. has implemented a whole-Teflon normally closed valve, which had a 1.4-mm diameter chamber with obstacle width of 250 μm [45]. The valve was able to block liquid flows with pressures within the range of 0.7-2.9 psi using a 14.5-psi actuation pressure. However, the negative pressure needed to open the valve was not mentioned. Simone et al. used Elastosil® membrane in combination with PMMA substrates to implement a normally closed valve with a diameter of 10 mm [60]. They used a 14-psi actuation pressure to obstruct liquid flows with a pressure of 4 psi. Grover et al. was able to bond Teflon membrane to glass substrates to implement an elliptical normally closed valve with a size of $1.2 \times 1.8$ mm$^2$ [61]. Characterizations revealed that the valve could block liquid flows with a pressure of approximately 7 psi using a 7.25-psi actuation pressure while it was completely open using an actuation pressure of approximately −10 psi. As explained earlier, the first trial to implement thermoplastic microvalve traced back to bonding of thermoplastic substrates to PDMS membrane such as that implemented by Zhang et al. in 2009 [35]. They fabricated a normally closed valve, which was able to stop liquid flows with pressures lower than 6.25 psi using an actuation pressure of 3.6 psi, whereas with a −8.7 psi of actuation pressure and a +8.7 psi of liquid pressure the valve was open with a liquid flow rate of approximately 924 μL/min. Implementation of whole-glass normally open microvalve using ultrathin (6-μm) glass membrane was demonstrated by Tanaka [62]. This glass valve had a circular structure with 3 mm in diameter and was able to block liquid flows up to 0.43 psi using actuation pressure of approximately 9.3 psi. Yalikun and Tanaka improved this work and implemented large-scale integration of whole-glass microvalves by a $10 \times 11$ valve array using the similar fabrication technology with 1.5-mm diameter microvalves and a 4-μm ultrathin glass membrane [63]. However, its fabrication technology is more expensive and complex than whole-thermoplastic microfluidic chips and they used a temperature of over 700 °C for bonding the layers. Grover et al. proposed the use of a 254-μm-thick PDMS membrane (HT-6240) in combination with glass substrates to implement normally closed

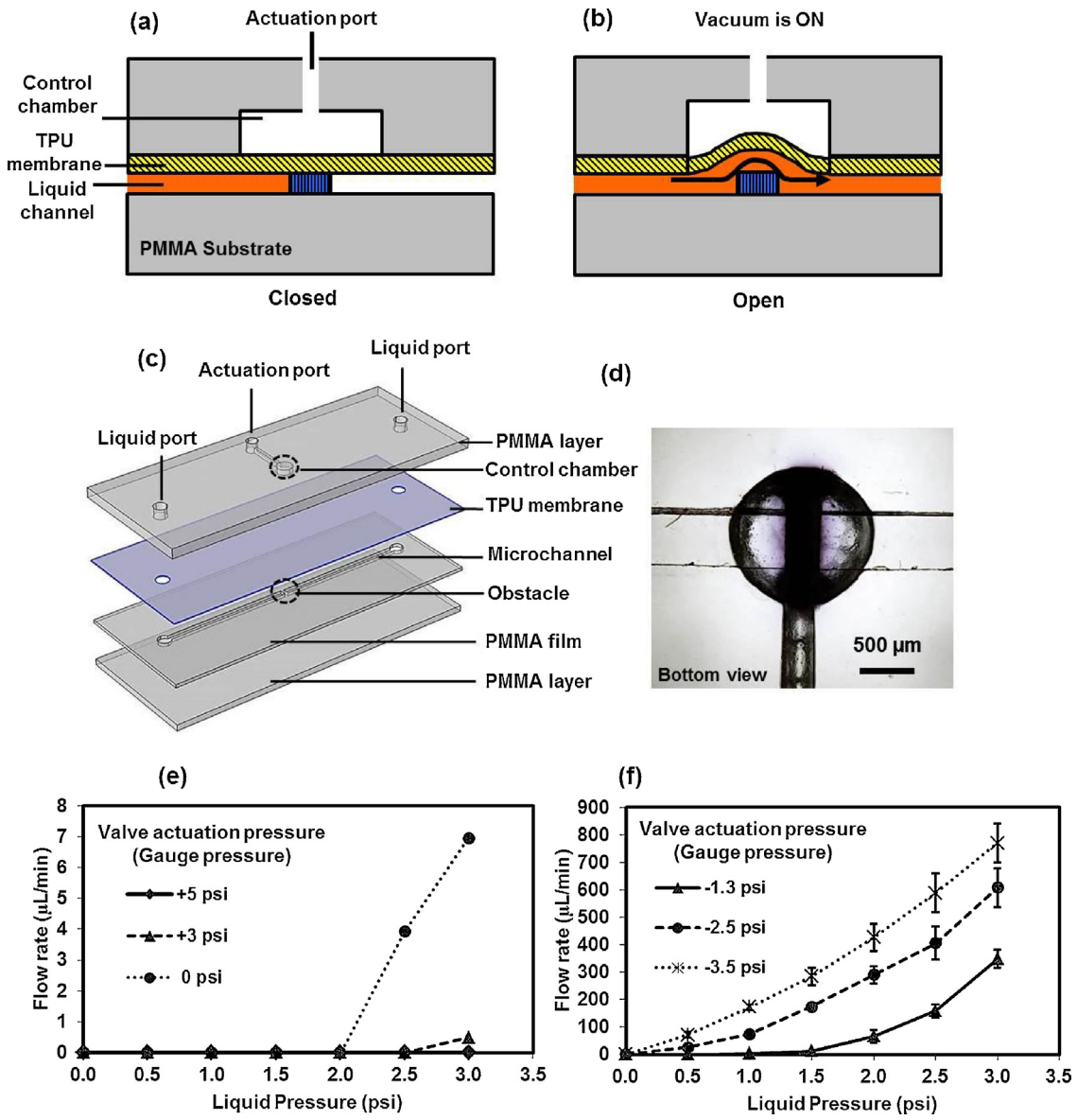


**Fig. 3.** Design and characterization of the normally closed microvalve. Schematics of the operation of the valve, (a) open, (b) closed, and (c) exploded view of the valve architecture. (d) Image showing a fabricated chip under microscope. (e) and (f) Characterization of the valve operation versus different liquid pressures and actuation pressures.

valve for use in microfluidic devices [64]. The valve had a different design with respect to our work and had a larger fluidic resistance. The microchannels of this work had a 100-μm width and a 40-μm depth with a circular valve chamber diameter of 1.5 mm. With an actuation pressure of −4.35 psi, the valve was completely open and flow rates of 3 μL/min up to 22.8 μL/min were measured while liquid pressure increased from 1.45 psi to 4.35 psi. At last, with actuation pressures of 1.45 psi and 6.5 psi, the valve could obstruct liquid flows with pressures of 5.8 psi and 10.8 psi, respectively.

It is obvious that in comparison to other whole-thermoplastic normally closed valves, the actuation pressure for blocking liquid flow in the current work is much lower. This can be associated with low thickness and material properties of the TPU membrane. Also, the fabrication process is more straightforward and economical [43–45].

### 3.2. Characterizations of the micro-check valve

Check valve, or one-way valve, is the hydraulic analog to the electronic diode in which it can allow liquid to pass only in one direction [65]. It is strongly required for lab-on-a-chip systems to avoid backflow and undesired introduction and mixing of different liquid streams. In general, fabrication of membrane-based micro-check valves using PDMS and soft lithography can be a challenging process since there is a need to generate multiple holes on a very thin PDMS membrane. This task requires accurate punching and alignment processes that are tedious and time-consuming especially for devices requiring many through-holes on the membrane [65–67]. This issue was resolved in our fabrication method by generating holes on the TPU film using the laser machining, which is rapid and scalable. Fig. 4a and b show the check valve functions in its reverse and forward modes, respectively. In the reverse mode, the check valve blocks liquid flow while in the forward mode, it allows the liquid to pass through the channel once its pressure reaches above a specific threshold. Schematic, photograph, and micrographs of the architecture of a fabricated check valve implemented within a whole-thermoplastic chip are shown in Fig. 4c–f.

The characterization experiments showed that the fabricated check valve could withstand a maximum pressure of 30 psi in the

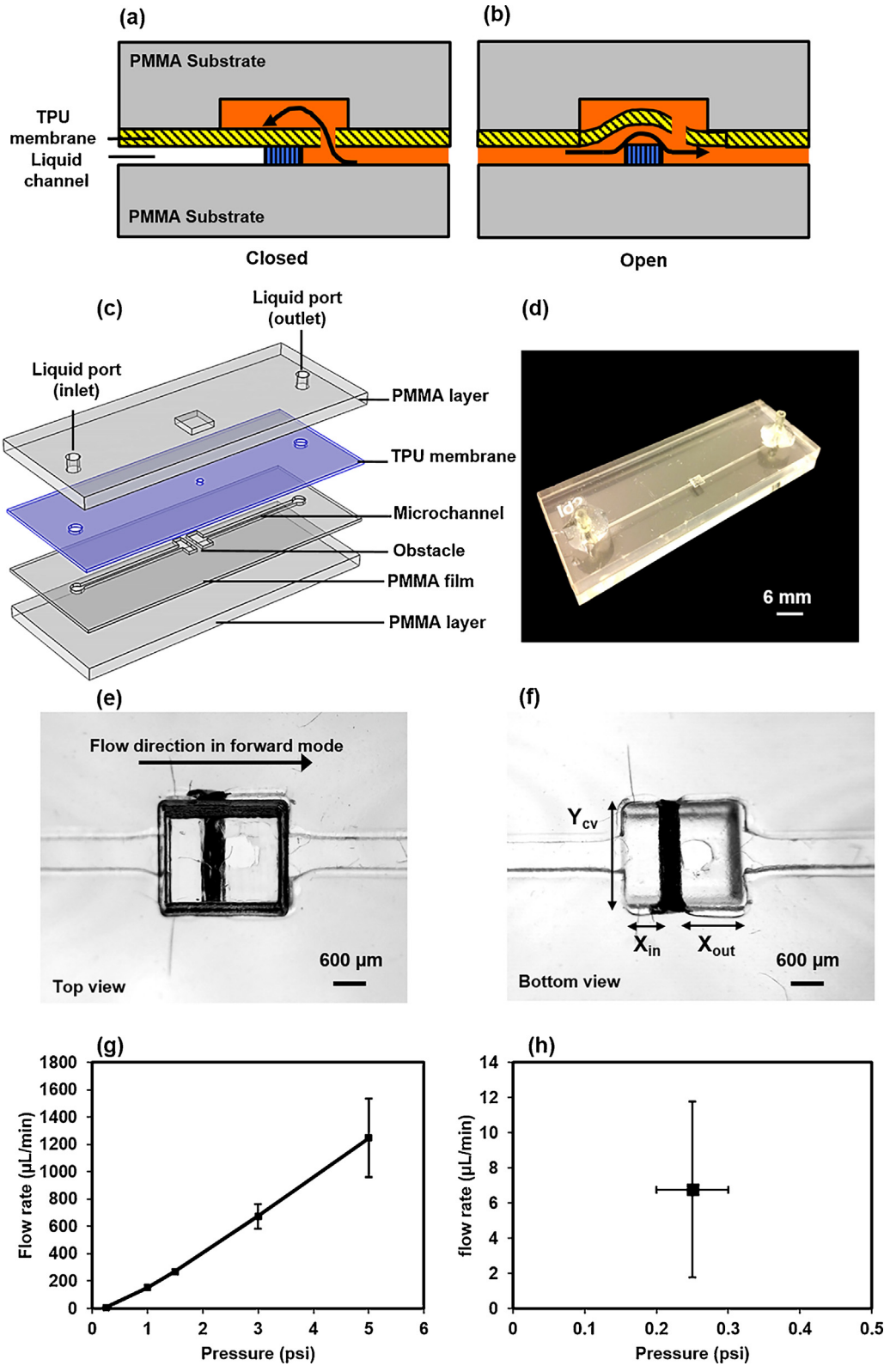


**Fig. 4.** Check valve operation, fabrication and characterization. Schematics showing (a) reverse mode and (b) forward mode, and (c); exploded view. (d) Photograph showing a fabricated chip. (e) Images showing top view of check valve chamber section under microscope and (f) bottom view of chamber section under microscope with dimensions. (g) Check valve leakage rate versus liquid pressure in forward mode; (h) pressure threshold of leakage for the fabricated check valves.

reverse mode without any leakage under a 24-h test. No burst leakage and failure in the bonding of the layers due to high liquid pressure was observed, which could be attributed to the high bonding strength. By swapping the inlet and outlet ports and exerting a negative pressure of −12 psi to the inlet, no leakage flow from the outlet towards the inlet was observed. However, by applying a positive pressure to the inlet, the check valve was switched to the forward mode leading to passage of the fluid through the check

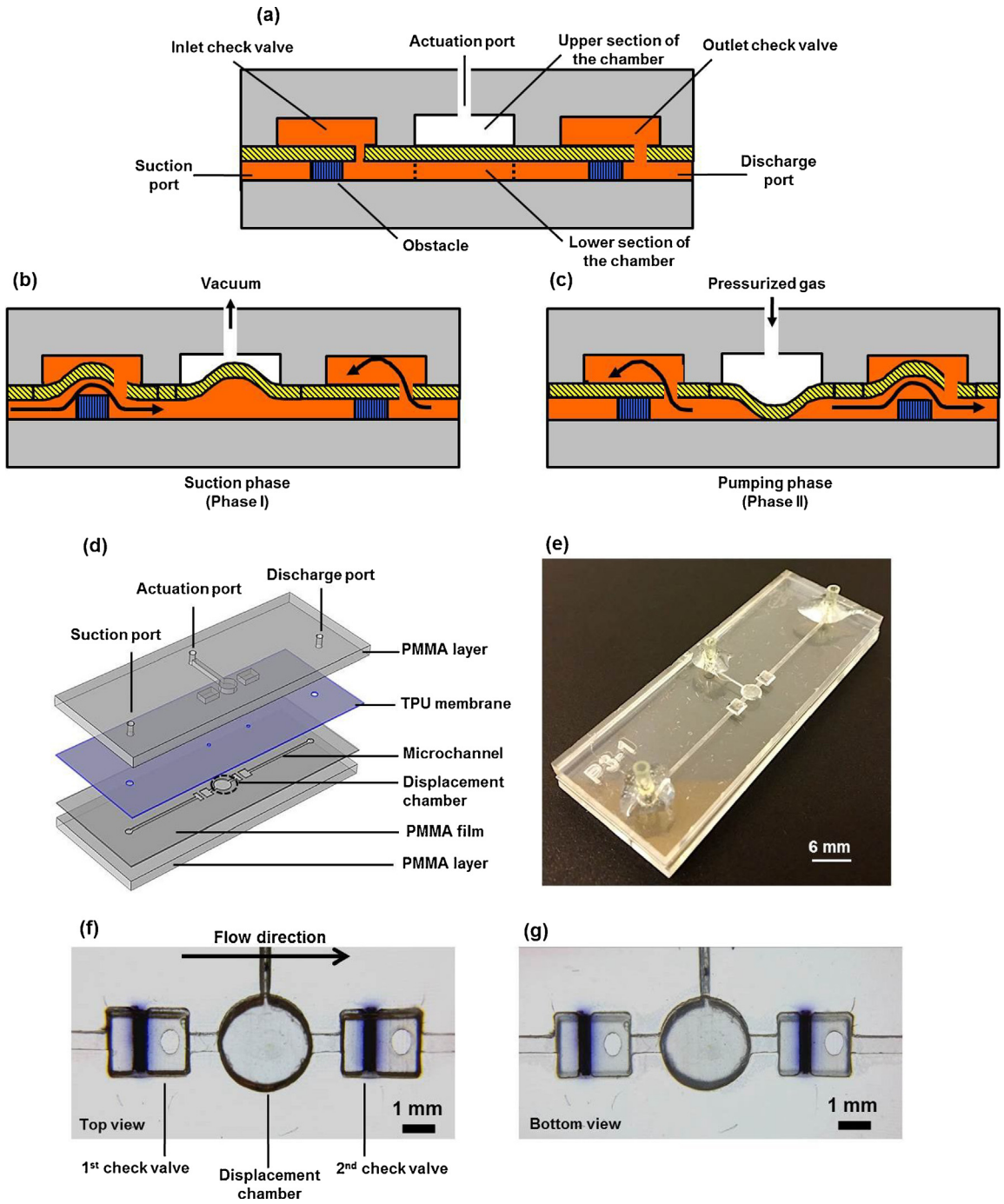


**Fig. 5.** Micropump operation and fabrication. Schematics showing (a) different sections of the pump, (b) suction phase, (c) pumping phase and (d) exploded view. (e) Photograph showing a fabricated chip (f) and (g) Images showing top and bottom views of the fabricated pump under microscope.

valve. As depicted in Fig. 4g, the flow rate increased almost linearly with respect to the increment of inlet liquid pressure. Further investigations revealed that the pressure threshold of the check valve, to initiate liquid flow, was approximately $0.25 \pm 0.05$ psi with an associated flow rate of $6.5 \pm 5.5$ μL/min (Fig. 4h). Threshold in the forward mode is dependent on the membrane mechanical properties and the size of the obstacle and the chamber. Any variations in the size of the obstacle and the chamber during the fabrication process can influence the value of the threshold. According to Fig. 4f, decreasing the membrane surface area ($A = X_{in} \times Y_{CV}$) increased the threshold pressure, because the amount of applied force by the liquid pressure to push up the membrane was decreased. Thus, the variation of the threshold point (Fig. 4h) in different chips might be due to a combination effect of precise control of gas pressure for liquid injection and fabrication errors, while variation in the flow rate at an inlet pressure of 5 psi (Fig. 4g) was mainly due to measurement errors.

Ball et al. implemented an out-of-plane flap-based check valve using a seven-layer structure (three adhesive layers, one Durometer silicon sheet, one planar PMMA or polyethylene terephthalate (PET) spring in combination with two PMMA substrates), and fabricated several valves with five different spring designs [68]. All

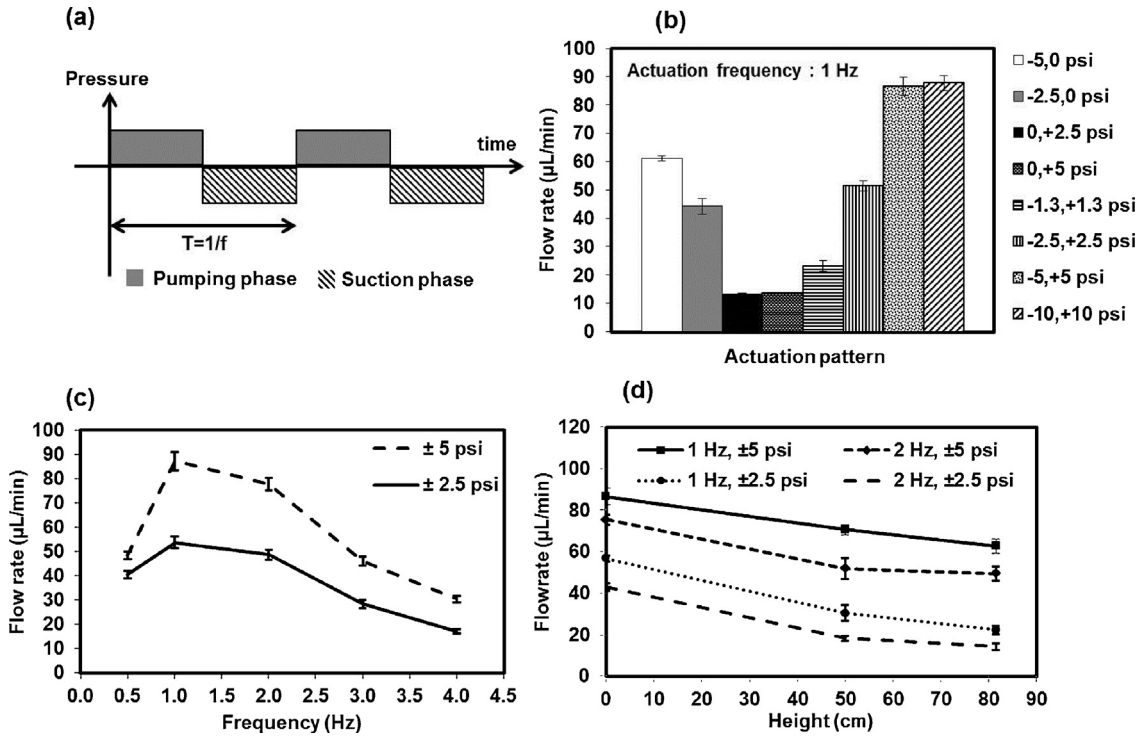


**Fig. 6.** Micropump characterization results. (a) Pump actuation phases. (b) Pumping flow rate versus different actuation pressures; negative and positive pressures are related to suction and pumping phases, respectively [suction pressure, pumping pressure]. (c) Pumping flow rate versus actuation frequency. (d) Pumping flow rate versus varying backpressures with different actuation pressures and frequencies.

of the designs had a total spring diameter of 5.5 mm. Experiments showed that, when springs were fabricated from the 200-μm-thick PMMA film, the valve threshold pressure in the forward mode was in the range of 5.8–25 psi depending on the design of the spring. However, when springs were fabricated from the 130-μm-thick PET film, the valve opening threshold was in the range of 0.7-8.0 psi depending of the design of the spring. To prevent the valve from back flows in the reverse mode, a soft and easily deformable 10A silicon sheet was used under the spring. As such, the valves could withstand back pressures of up to 40 psi in the reverse mode, depending on the spring design. In comparison, the implemented whole-thermoplastic membrane-based check valve in the current report is much simpler and practical for lab-on-a-chip applications than previously reported check valves [68].

Mosadegh et al. implemented a series of membrane-based PDMS check valves with geometry similar to that shown in Fig. 4f of our study, using a 30-μm PDMS membrane, a 300-μm wide obstacle, but with different width and length [67,69]. All of the valves reported in [67,69] were able to withstand back pressures of up to 45 psi for at least 1 h. Characterization tests of forward mode revealed that the threshold pressures for components with a constant width of 1 mm and lengths ($X_{in}$ of Fig. 4f) of 800, 400, and 200 μm were approximately 1.5, 2.6, and 3.3 psi, respectively. Ni et al. [70] improved their previous design [71] and implemented a PDMS in-plane flap-based check valve and pump (the pump will be compared in the next section). Its flexible flap (250-μm long and 40-μm wide) was vertically fixed to one sidewall of the microchannel (300-μm wide and 300-μm high) with a 20-μm distance to the stopper while the rigid stopper sat to both sidewalls separated by a centered stopper channel (400-μm long and 60-μm wide). The valve could allow the liquid to pass with a flow rate of 1600 μL/min at a forward pressure of 4.35 psi. However, in the reverse mode, with the liquid pressures of 0.7–4.35 psi the valve had a constant leakage flow rate of 50 μL/min.

### 3.3. Micropump characterizations

Several efforts have been reported to implement check valve micropumps on various materials with different actuation methods. In the past decade, such microfluidic systems have been widely realized on silicon-based substrates with piezoelectric actuation [66,72,73]. Kim et al. implemented a check valve micropump on PDMS using two flap-based check valves with pneumatic actuation [74] and studied pulsatile nature of liquid flow on cells [75]. Combination of PMMA and PDMS with piezoelectric actuation for micropumping has also been reported [76–78]. We have specifically implemented a whole-thermoplastic micropump with pneumatic actuation by the integration of two membrane-based check valves with a uni-diaphragm displacement chamber on a single liquid channel (Fig. 5). In the current design of the micropump, the depth of the check valves was designed to be about 250 μm while the circular displacement chamber had a depth of about 600 μm with a diameter of 3 mm. This architecture allowed for decreasing the dead volume of liquid entrapped between inlet check valve and the displacement chamber. The volumes of the upper and lower sections of the chamber were approximately 4.24 μL and 0.88 μL, respectively, while the volume of the check valves was approximately 1.00 μL (Fig. 5a).

The micropump function consists of suction and pumping phases (strokes), as shown in Fig. 6a. During the suction phase, vacuum is applied to the actuation chamber causing liquid to be drawn into the displacement chamber through the suction port. In this phase, liquid can pass through the check valve from the suction port while the check valve at the discharge port stops the liquid flow. During the pumping phase, the actuation chamber is pressurized pushing liquid to the discharge port. In this phase of operation, the check valve at the suction port is in its reverse mode of function and blocks liquid flow while the check valve at the discharge port allows the liquid to pass through the microchannel (Fig. 5b and c).

Thus, the check valve micropump generates a pulsatile flow rate pattern with the same frequency at which it is actuated.

Response of the micropump against various actuation pressures and frequencies was characterized (Fig. 6b–c). During all the tests, the inlet of the suction port and the outlet of the discharge port were located at the same height. Fig. 6b shows the effect of the actuation pattern (symmetric and asymmetric) on the pumping flow rate. For all the tests, the actuation frequency was set at 1 Hz with duty cycle of 50% each. It was shown that a flow rate of 60 μL/min was produced using actuation pressures of −5 psi (at suction phase) and 0 psi (at pumping phase), i.e. (−5 psi, 0 psi), while a flow rate of 44 μL/min was produced by employing pressures of (−2.5 psi, 0 psi). The minimum pumping flow rate (13.4 ± 0.4 μL/min) was produced at pressures of (0 psi, +2.5 psi) and (0 psi, +5 psi) while the maximum pumping flow rates of 86.6 ± 5.0 μL/min and 87.6 ± 5.0 μL/min were produced at the symmetrical actuation pressures of ±5 psi and ±10 psi, respectively. When the pump is actuated using the asymmetric pattern, spring property of the membrane is the only force to return the membrane to its initial position. For positive asymmetric pressures (0, +2.5 psi) and (0, +5 psi), the pump only uses the lower section of the displacement chamber. In contrary, for negative actuation pressures of (−5 psi, 0 psi) and (−2.5 psi, 0 psi), the pump uses the upper section of the chamber for pumping, which contains a larger volume, thus achieving a higher flow rate. Further characterizations revealed that the total pumping flow rate was improved through the use of symmetrical actuation pressures, e.g. ±5 psi and ±10 psi, with the application of negative pressure during the suction phase (phase I) and positive pressure for the pumping phase (phase II). The positive actuation in the symmetric pattern helps the membrane to push the fluid to the discharge port. Thus, higher positive pressures can overcome higher backpressures at the outlet.

The effect of actuation frequency on the pumping flow rate was further studied. Fig. 6c indicates that there was an optimum frequency of actuation for maximum flow rate of pumping. Once the frequency was increased to 1 Hz, maximum pumping flow rates of 51 ± 3.0 μL/min and 89 ± 6.0 μL/min for actuation pressures of ±2.5 psi and ±5 psi were obtained, respectively. The stroke volumes (displacement volumes) for ±2.5 psi and ±5 psi actuation pressures were 2000 nL and 2400 nL, respectively, which were calculated using numerical simulations (COMSOL Multiphysics). However, the average measured pumping volumes for ±2.5 psi and ±5 psi actuation pressures (while the actuation frequency was 0.5 Hz in both cases) were 1290 ± 40 nL/stroke and 1560 ± 40 nL/stroke, respectively. The minimum measured pumping volumes for ±2.5 psi and ±5 psi actuation pressures (while the actuation frequency was 4 Hz in both cases) were 80 ± 5 nL/stroke and 125 ± 5 nL/stroke, respectively. This difference can be result of several affecting parameters including, liquid entrapment between the inlet check valve and pump chamber, probable bubble entrapment in the check-valve chambers and microchannels, pressure drop at the discharge port of the pump, as well as pump actuation frequency [72]. Obviously, the pump performance may be improved if the diameter of the pumping chamber increases.

Since the pump exhibited negative pressure (in suction phase) at the inlet, it showed self-priming property and could suck the liquid from reservoir to the chip while the tubing and microchannels were empty of liquid. This capability is of particular importance for certain on-chip applications where the microfluidic chip is initially empty of liquid and the liquid should be pumped through from a reservoir using a built-in micropump. The operation of the micropump can be observed in the supplementary video (ESI: Movie S1).

For further characterization of the micropump, the correlation of resistive pressure against the flow at the outlet port (backpressure) and the pumping flow rate was investigated (Fig. 6d). Tubing with an inner diameter of 508 μm was connected vertically to the outlet of the pump discharge port and filled with water to create a liquid column with certain height and backpressure. The flow rate was measured at different heights of the liquid column. It was revealed that the flow rate declined for all patterns of actuation when the height of the liquid column increased from 0 to 81 cm, which is equivalent to a backpressure of 1.15 psi, (Fig. 6d). For actuation frequency of 1 Hz and actuation pressure of ±5 psi, the flow rate dropped from 86 ± 4.0 μL/min to 42 ± 2.0 μL/min as the backpressure increased from 0 to 2.1 psi, which is equivalent to height of 150 cm. We were only able to measure up to heights of 150 cm due to constraints in the laboratory, while the actuation frequency and pressure were 1 Hz and ±5 psi, respectively. However, since these types of pump usually have linear responses to backpressures [71,79,80], we concluded (by calculations from Fig. 6d) that our pump could withstand a backpressure of approximately 4.4 psi, which is equivalent to height of 310 cm.

The fabricated micropump had dimensions of $9.3 \times 3 \times 3\ mm^3$ (without considering the side channels). Our method of whole-thermoplastic micropump fabrication is much easier than the one used for micropumps implemented in PMMA substrate and PDMS membrane with piezoelectric actuation for liquid pumping [76,77]. The reported devices had dimensions of $20 \times 20 \times 28\ mm^3$, fabricated in 10 layers. Experimental results [76] showed that the maximum flow rate of 118 mL/min was obtained using a sinusoidal voltage of 60 V at 361 Hz for pumping. Conde et al. have also implemented another piezoelectric actuated check valve micropump ($22 \times 11 \times 2.2\ mm^3$) in which they used three PMMA layers in combination with two PDMS O-ring diaphragms to implement the pump [81]. Maximum average flow rate of 120 μL/min was obtained with a backpressure of about 1.4 psi while it was driven by a sinusoidal voltage of 100 V at 120 Hz.

Ni et al. reported a PDMS micropump using a 150-μm thick membrane and two flap-based check valves [71]. The diameter and height of the pump chamber were 4.4 mm and 200 μm, respectively. The maximum flow rates of 19.3 μL/min, 25.8 μL/min, and 41.0 μL/min were obtained under the pneumatic pressure amplitudes of 4.35 psi, 6.5 psi, and 8.7 psi at zero back pressure, respectively, at the actuation frequency of 2 Hz. The zero flow rate pressure head of the pump was approximately 3.6 psi at an actuation frequency of 2 Hz and an actuation pressure of 6.5 psi. The total chip size was about $10 \times 10\ mm^2$. Grover et al. fabricated several three-layer glass/PDMS/glass micropumps using a combination of three normally closed valves in a way that the middle valve had larger area and worked similar to the displacement chamber while the other valves actuated in a way that they worked similar to check valves [64]. The pumps were self-priming and were able to pump from 0.06 μL/min to over 6 μL/min (according to their size) while the pumps were actuated at −11.6 psi and +5.8 psi pressures. The pumps were able to pump approximately 82% of the chamber volume per cycle. According to the data provided in this report it is reasonable to conclude that a device with a 20 μm depth fluid layer, a 70 μm etch depth of chamber, and a chamber diameter of 3 mm (which had a volume of 0.531 μL) and at optimum actuation time (0.5 Hz), could pump flow rate of maximally 3 μL/min at zero back pressure. When the chamber diameter was 1.5 mm and at its optimum actuation time, the maximum flow rate of 1.8 μL/min and 0.78 μL/min were attained at backpressure of 2.9 psi and 4.35 psi, respectively.

## 4. Conclusions

In this paper, we described the fabrication of three types of fundamental microfluidic actuators including a normally closed microvalve, a micro-check valve, and a dual-phase micropump. The whole-thermoplastic actuators were fabricated employing laser-

micromachined PMMA sheets and TPU films assembled through thermal fusion bonding. The developed fabrication method is straightforward and inexpensive with rapid processing time in comparison with thermoforming and hot embossing methods [50]. These features make the developed fabrication method appropriate for rapid chip fabrication in academic settings for chemical and biological applications. Using laser-machining method to create microfluidic architectures eliminated the use of any master mold for patterning purposes, which is commonly used for creating features on thermoplastic-based microfluidics [45,49]. In addition, the developed fabrication process does not require any chemical treatment, plasma or UV/ozone exposure for bonding as used for some thermoplastic chip fabrication [44,49]. The presented fabrication method has fewer steps compared to the reported fabrication methods [45,49,82]. The normally closed microvalve could stop liquid flow in its passive mode for liquid pressures of up to 2 psi as no actuation pressure was used. The micro-check valve could provide leakage-free operations in its reverse mode for liquid pressures of up to 30 psi. Furthermore, the pneumatic-actuated micropump could demonstrate a successful continual operation with constant average flow rate of 87.6 μL/min at an actuation pressure and frequency of ±5 psi and 1 Hz, respectively, which is sufficient for a vast majority of microfluidic and on-chip applications. For future improvements, the dimensions of the fabricated devices can be downsized and the quality of the laser micromachining can be improved by fine tuning of laser properties. Miniaturization can be achieved with enhanced control over the operation of the devices with higher density of on-chip integration. Also, the minimum pumping flow rate of the micropump can be reduced through optimization and downsizing processes for applications require high-resolution control over low flow rates. More precise control over the thermal bonding process may be achieved using customized metallic jigs with controllable bonding pressure.

## Acknowledgments

The authors acknowledge funding from the National Institutes of Health (AR057837, AR066193, EB022403, EB021148, HL137193, EB021857, AR070647, EB023052, CA214411, and EB024403) and the Presidential Early Career Award for Scientists and Engineers (PECASE). Y.S.Z. acknowledges funding from the National Cancer Institute of the National Institutes of Health (CA201603), the Lush Prize, and the Science and Technology Commission of Shanghai Municipality (STCSM) 17JC 1400200.

## Appendix A. Supplementary data

Supplementary data associated with this article can be found, in the online version, at https://doi.org/10.1016/j.snb.2017.12.132.

## References

[1] D. Voicu, et al., Thermoplastic microfluidic devices for targeted chemical and biological applications, RSC Adv. 7 (5) (2017) 2884–2889.
[2] E.K. Sackmann, A.L. Fulton, D.J. Beebe, The present and future role of microfluidics in biomedical research, Nature 507 (7491) (2014) 181–189.
[3] K.M. Weerakoon-Ratnayake, C.E. O'Neil, F.I. Uba, S.A. Soper, Thermoplastic nanofluidic devices for biomedical applications, Lab Chip 17 (2017) 362–381.
[4] E. Berthier, E.W. Young, D. Beebe, Engineers are from PDMS-land, biologists are from polystyrenia, Lab Chip 12 (7) (2012) 1224–1237.
[5] E. Berthier, J. Warrick, H. Yu, D.J. Beebe, Managing evaporation for more robust microscale assays Part 1. Volume loss in high throughput assays, Lab Chip 8 (6) (2008) 852–859.
[6] M.H. Wu, G. Dimopoulos, A. Mantalaris, J. Varley, The effect of hyperosmotic pressure on antibody production and gene expression in the GS-NS0 cell line, Biotechnol. Appl. Biochem. 40 (1) (2004) 41–46.
[7] R. Kimura, W.M. Miller, Effects of CO2 and osmolality on hybridoma cells: growth, metabolism and monoclonal antibody production, in: Cell Culture Engineering VI, Springer, 1998.
[8] K.J. Regehr, et al., Biological implications of polydimethylsiloxane-based microfluidic cell culture, Lab Chip 9 (15) (2009) 2132–2139.
[9] M.W. Toepke, D.J. Beebe, PDMS absorption of small molecules and consequences in microfluidic applications, Lab Chip 6 (12) (2006) 1484–1486.
[10] J.N. Lee, C. Park, G.M. Whitesides, Solvent compatibility of poly (dimethylsiloxane)-based microfluidic devices, Anal. Chem. 75 (23) (2003) 6544–6554.
[11] D.I. Walsh, D.S. Kong, S.K. Murthy, P.A. Carr, Enabling microfluidics: from clean rooms to makerspaces, Trends Biotechnol. 35 (2017) 383–392.
[12] C.-W. Tsao, D.L. DeVoe, Bonding of thermoplastic polymer microfluidics, Microfluid. Nanofluid. 6 (1) (2009) 1–16.
[13] G. Khanarian, H. Celanese, Optical properties of cyclic olefin copolymers, Opt. Eng. 40 (6) (2001) 1024–1029.
[14] H. Becker, L.E. Locascio, Polymer microfluidic devices, Talanta 56 (2) (2002) 267–287.
[15] L. Martynova, L.E. Locascio, M. Gaitan, G.W. Kramer, R.G. Christensen, W.A. MacCrehan, Fabrication of plastic microfluid channels by imprinting methods, Anal. Chem. 69 (23) (1997) 4783–4789.
[16] R.M. McCormick, R.J. Nelson, M.G. Alonso-Amigo, D.J. Benvegnu, H.H. Hooper, Microchannel electrophoretic separations of DNA in injection-molded plastic substrates, Anal. Chem. 69 (14) (1997) 2626–2630.
[17] J. Giboz, T. Copponnex, P. Mélé, Microinjection molding of thermoplastic polymers: a review, J. Micromech. Microeng. 17 (6) (2007) R96.
[18] T.-F. Hong, W.-J. Ju, M.-C. Wu, C.-H. Tai, C.-H. Tsai, L.-M. Fu, Rapid prototyping of PMMA microfluidic chips utilizing a CO2 laser, Microfluid. Nanofluid. 9 (6) (2010) 1125–1133.
[19] H. Li, Y. Fan, R. Kodzius, I.G. Foulds, Fabrication of polystyrene microfluidic devices using a pulsed CO2 laser system, Microsyst. Technol. 18 (3) (2012) 373–379.
[20] J.-H. Lee, E.T. Peterson, G. Dagani, I. Papautsky, Rapid prototyping of plastic microfluidic devices in cyclic olefin copolymer (COC), in: MOEMS-MEMS Micro & Nanofabrication, International Society for Optics and Photonics, 2005, pp. 82–91.
[21] H. Zhang, X. Liu, T. Li, X. Han, Miscible organic solvents soak bonding method use in a PMMA multilayer microfluidic device, Micromachines 5 (4) (2014) 1416–1428.
[22] H. Shadpour, et al., Multichannel microchip electrophoresis device fabricated in polycarbonate with an integrated contact conductivity sensor array, Anal. Chem. 79 (3) (2007) 870–878.
[23] J.P. Grinias, R.T. Kennedy, Advances in and prospects of microchip liquid chromatography, TrAC Trends Anal. Chem. 81 (2016) 110–117.
[24] R. Jellali, P. Paullier, M.-J. Fleury, E. Leclerc, Liver and kidney cells cultures in a new perfluoropolyether biochip, Sens. Actuators, B 229 (2016) 396–407.
[25] L.X. Kong, K. Parate, K. Abi-Samra, M. Madou, Multifunctional wax valves for liquid handling and incubation on a microfluidic CD, Microfluid. Nanofluid. 6 (2015) 1031–1037.
[26] D.S. Kim, H.S. Lee, J. Han, S.H. Lee, C.H. Ahn, T.H. Kwon, Collapse-free thermal bonding technique for large area microchambers in plastic lab-on-a-chip applications, Microsyst. Technol. 14 (2) (2008) 179–184.
[27] M. La, et al., A centrifugal force-based serpentine micromixer (CSM) on a plastic lab-on-a-disk for biochemical assays, Microfluid. Nanofluid. 15 (1) (2013) 87–98.
[28] S. Zehnle, F. Schwemmer, G. Roth, F. von Stetten, R. Zengerle, N. Paust, Centrifugo-dynamic inward pumping of liquids on a centrifugal microfluidic platform, Lab Chip 12 (24) (2012) 5142–5145.
[29] M.M. Aeinehvand, et al., Biosensing enhancement of dengue virus using microballoon mixers on centrifugal microfluidic platforms, Biosens. Bioelectron. 67 (2015) 424–430.
[30] A.K. Au, N. Bhattacharjee, L.F. Horowitz, T.C. Chang, A. Folch, 3D-printed microfluidic automation, Lab Chip 15 (8) (2015) 1934–1941.
[31] A.K. Au, W. Lee, A. Folch, Mail-order microfluidics: evaluation of stereolithography for the production of microfluidic devices, Lab Chip 14 (7) (2014) 1294–1301.
[32] R. Amin, et al., 3D-printed microfluidic devices, Biofabrication 8 (2) (2016) 022001.
[33] A.K. Au, W. Huynh, L.F. Horowitz, A. Folch, 3D-printed Microfluidics, Angewandte Chemie International Edition, 2016.
[34] R. Sochol, et al., 3D printed microfluidic circuitry via multijet-based additive manufacturing, Lab Chip 16 (4) (2016) 668–678.
[35] W. Zhang, et al., PMMA/PDMS valves and pumps for disposable microfluidics, Lab Chip 9 (21) (2009) 3088–3094.
[36] P. Gu, K. Liu, H. Chen, T. Nishida, Z.H. Fan, Chemical-assisted bonding of thermoplastics/elastomer for fabricating microfluidic valves, Anal. Chem. 83 (1) (2010) 446–452.
[37] K. Liu, P. Gu, K. Hamaker, Z.H. Fan, Characterization of bonding between poly (dimethylsiloxane) and cyclic olefin copolymer using corona discharge induced grafting polymerization, J. Colloid Interface Sci. 365 (1) (2012) 289–295.
[38] Z.H. Fan, P. Gu, S. Augustine, K. Liu, H. Freitag, T. Nishida, Microfluidic valve arrays in thermoplastic devices, in: ASME 2012 10th International Conference on Nanochannels, Microchannels, and Minichannels, Rio Grande, Puerto Rico, USA, ASME. ICNMM2012-73021, 2012, pp. 453–458.
[39] O. Cybulski, S. Jakiela, P. Garstecki, Whole Teflon valves for handling droplets, Lab Chip 16 (12) (2016) 2198–2210.

[40] Z. Zhang, Z. Zhu, N. Xiang, H. Yi, Inexpensive, rapid fabrication of polymer-film microfluidic autoregulatory valve for disposable microfluidics, Biomed. Microdevices 19 (2) (2017) 21.
[41] C.I. Rogers, J.B. Oxborrow, R.R. Anderson, L.-F. Tsai, G.P. Nordin, A.T. Woolley, Microfluidic valves made from polymerized polyethylene glycol diacrylate, Sens. Actuators B: Chem. 191 (2014) 438–444.
[42] V. Sunkara, D.-K. Park, H. Hwang, R. Chantiwas, S.A. Soper, Y.-K. Cho, Simple room temperature bonding of thermoplastics and poly (dimethylsiloxane), Lab Chip 11 (5) (2011) 962–965.
[43] P. Zhou, L. Young, Z. Chen, Weak solvent based chip lamination and characterization of on-chip valve and pump, Biomed. Microdevices 12 (5) (2010) 821–832.
[44] I. Ogilvie, V. Sieben, B. Cortese, M. Mowlem, H. Morgan, Chemically resistant microfluidic valves from Viton® membranes bonded to COC and PMMA, Lab Chip 11 (14) (2011) 2455–2459.
[45] K. Ren, W. Dai, J. Zhou, J. Su, H. Wu, Whole-Teflon microfluidic chips, Proc. Natl. Acad. Sci. 108 (20) (2011) 8162–8166.
[46] C. Hu, et al., A one-step strategy for ultra-fast and low-cost mass production of plastic membrane microfluidic chips, Lab Chip 16 (20) (2016) 3909–3918.
[47] J.P. Rolland, R.M. Van Dam, D.A. Schorzman, S.R. Quake, J.M. DeSimone, Solvent-resistant photocurable liquid teflon for microfluidic device fabrication, J. Am. Chem. Soc. 126 (8) (2004) 2322–2323.
[48] J.P. Rolland, E.C. Hagberg, G.M. Denison, K.R. Carter, J.M. De Simone, High-resolution soft lithography: enabling materials for nanotechnologies, Angew. Chem. Int. Ed. 43 (43) (2004) 5796–5799.
[49] P. Gu, T. Nishida, Z.H. Fan, The use of polyurethane as an elastomer in thermoplastic microfluidic devices and the study of its creep properties, Electrophoresis 3 (2014) 289–297.
[50] E. Roy, J.-C. Galas, T. Veres, Thermoplastic elastomers for microfluidics: towards a high-throughput fabrication method of multilayered microfluidic devices, Lab Chip 11 (18) (2011) 3193–3196.
[51] E. Piccin, W.K.T. Coltro, J.A.F. da Silva, S.C. Neto, L.H. Mazo, E. Carrilho, Polyurethane from biosource as a new material for fabrication of microfluidic devices by rapid prototyping, J. Chromatogr. A 1173 (1) (2007) 151–158.
[52] W.-I. Wu, K.N. Sask, J.L. Brash, P.R. Selvaganapathy, Polyurethane-based microfluidic devices for blood contacting applications, Lab Chip 12 (5) (2012) 960–970.
[53] S.A.M. Shaegh, et al., Plug-and-play microvalve and micropump for rapid integration with microfluidic chips, Microfluid. Nanofluid. 19 (3) (2015) 557–564.
[54] S.A.M. Shaegh, et al., Rapid prototyping of whole-thermoplastic microfluidics with built-in microvalves using laser ablation and thermal fusion bonding, Sens. Actuators, B 255 (Part 1) (2018) 100–109.
[55] M.V. Pergal, et al., Structure and properties of thermoplastic polyurethanes based on poly (dimethylsiloxane): assessment of biocompatibility, J. Biomed. Mater. Res. A 102 (11) (2014) 3951–3964.
[56] Y.S. Zhang, et al., Multisensor-integrated organs-on-chips platform for automated and continual in situ monitoring of organoid behaviors, Proc. Natl. Acad. Sci. 114 (12 (March)) (2017) E2293–E2302.
[57] J. Melin, S.R. Quake, Microfluidic large-scale integration: the evolution of design rules for biological automation, Annu. Rev. Biophys. Biomol. Struct. 36 (2007) 213–231.
[58] R. Riahi, et al., Automated microfluidic platform of bead-based electrochemical immunosensor integrated with bioreactor for continual monitoring of cell secreted biomarkers, Sci. Rep. 6 (2016).
[59] S.R. Shin, et al., Label-free and regenerative electrochemical microfluidic biosensors for continual monitoring of cell secretomes, Adv. Sci. 4 (2017) 1600522.
[60] G. Simone, et al., A microvalve for hybrid microfluidic systems, Microsyst. Technol. 16 (7) (2010) 1269–1276.
[61] W.H. Grover, M.G. von Muhlen, S.R. Manalis, Teflon films for chemically-inert microfluidic valves and pumps, Lab Chip 8 (6) (2008) 913–918.
[62] Y. Tanaka, Electric actuating valves incorporated into an all glass-based microchip exploiting the flexibility of ultra thin glass, RSC Adv. 3 (26) (2013) 10213–10220.
[63] Y. Yalikun, Y. Tanaka, Large-scale integration of all-glass valves on a microfluidic device, Micromachines 7 (5) (2016) 83.
[64] W.H. Grover, A.M. Skelley, C.N. Liu, E.T. Lagally, R.A. Mathies, Monolithic membrane valves and diaphragm pumps for practical large-scale integration into glass microfluidic devices, Sens. Actuators, B 89 (3) (2003) 315–323.
[65] K.W. Oh, C.H. Ahn, A review of microvalves, J. Micromech. Microeng. 16 (5) (2006) R13.
[66] A.K. Au, H. Lai, B.R. Utela, A. Folch, Microvalves and micropumps for BioMEMS, Micromachines 2 (2) (2011) 179–220.
[67] B. Mosadegh, et al., Integrated elastomeric components for autonomous regulation of sequential and oscillatory flow switching in microfluidic devices, Nat. Phys. 6 (6) (2010) 433–437.
[68] C. Ball, R. Renzi, A. Priye, R. Meagher, A simple check valve for microfluidic point of care diagnostics, Lab Chip 16 (22) (2016) 4436–4444.
[69] B. Mosadegh, C. Kuo, Y. Tung, Y. -s. Torisawa, S. Takayama, A monolithic passive check-valve for systematic control of temporal actuation in microfluidic devices, in: Proceedings of the Twelfth International Conference on Miniaturized Systems for Chemistry and Life Sciences, San Diego, CA, USA, 2008, vol. 1216, p. 826828.
[70] J. Ni, B. Li, J. Yang, A pneumatic PDMS micropump with in-plane check valves for disposable microfluidic systems, Microelectron. Eng. 99 (2012) 28–32.
[71] J. Ni, F. Huang, B. Wang, B. Li, Q. Lin, A planar PDMS micropump using in-contact minimized-leakage check valves, J. Micromech. Microeng. 20 (9) (2010).
[72] D.J. Laser, J.G. Santiago, A review of micropumps, J. Micromech. Microeng. 14 (6) (2004) R35.
[73] G.-H. Feng, E.S. Kim, Micropump based on PZT unimorph and one-way parylene valves, J. Micromech. Microeng. 14 (4) (2004).
[74] J. Kim, et al., Photopolymerized check valve and its integration into a pneumatic pumping system for biocompatible sample delivery, Lab Chip 6 (8) (2006) 1091–1094.
[75] J. Kim, et al., A cell culturing system that integrates the cell loading function on a single platform and evaluation of the pulsatile pumping effect on cells, Biomed. Microdevices 10 (1) (2008) 11–20.
[76] X.Y. Wang, Y.T. Ma, G.Y. Yan, Z.H. Feng, A compact and high flow-rate piezoelectric micropump with a folded vibrator, Smart Mater. Struct. 23 (11) (2014) 115005.
[77] Y.-t. Ma, X.-y. Wang, J.-f. Zhong, Z.-h. Feng, Resonantly Driven Piezoelectric Micropump with PDMS Check Valves and Compressible Space, Piezoelectricity, Acoustic Waves, and Device Applications (SPAWDA), 2014 Symposium on 2014, IEEE, 2014, pp. 158–161.
[78] P. Zeng, L. a. Li, J. Dong, G. Cheng, J. Kan, F. Xu, Structure design and experimental study on single-bimorph double-acting check-valve piezoelectric pump, Proc. Inst. Mech. Eng. Part C: J. Mech. Eng. Sci. 230 (2015) 2339–2344, p. 0954406215596357.
[79] E. Meng, X.-Q. Wang, H. Mak, Y.-C. Tai, A check-valved silicone diaphragm pump, in: Micro Electro Mechanical Systems, 2000. MEMS 2000, The Thirteenth Annual International Conference on, 2000, IEEE, 2000, pp. 62–67.
[80] J. Kang, G.W. Auner, Simulation and verification of a piezoelectrically actuated diaphragm for check valve micropump design, Sens. Actuat. A: Phys. 167 (2) (2011) 512–516.
[81] A. Conde, et al., A polymer chip-integrable piezoelectric micropump with low backpressure dependence, RSC Adv. 5 (62) (2015) 49996–50000.
[82] S.A. Aghvami, et al., Rapid prototyping of cyclic olefin copolymer (COC) microfluidic devices, Sens. Actuators, B 247 (2017) 940–949.

## Biographies

**Adel Pourmand** received his M.Sc. degree in Electronic Engineering with focus on microelectromechanical systems and microfluidics from Sahand University of Technology (SUT) in 2011. He started his PhD program from 2012 at SUT to develop microfluidic-based cell/particle sorting methods and microfluidic fabrication technologies. In 2015, he joined Harvard-MIT Division of Health Sciences and Technology as a visiting PhD student to work on thermoplastic-based microfluidic devices. His research interests include development of MEMS-based sensors and actuators, microfluidics, lab-on-chip and organ-on-chip systems.

**Seyed Ali Mousavi Shaegh** received his Ph.D. in Mechanical Engineering on microfluidic power sources for portable applications from Nanyang Technological University in 2012. Subsequently, he joined Singapore Institute of Manufacturing Technologies as a research scientist to lead translation researches on the development of thermoplastic-based microfluidic devices for point-of-care diagnostics. In 2014, he joined Harvard-MIT Division of Health Sciences and Technology as a postdoctoral fellow where his research was mainly on design and fabrication of organ-on-chip platforms with integrated sensors for drug screening applications. Recently, he has joined Mashhad University of Medical Sciences as an Assistant Professor of Biomedical Engineering. His current research interests are mainly focused on microfluidic devices and sensing platforms for drug screening and point-of-care detections as well as design of medical devices and implants.

**Habib Badri Ghavifekr** received the BS degree from Tabriz University, Iran, and continued his study in Germany and received the MS degree from Technical University of Berlin, in 1995 both in electrical engineering. Subsequently, he joined the Institute for Microperipheric at the Technical University of Berlin as a scientific assistant and in 1998 the Fraunhofer Institute for Reliability and Microintegration as a research assistant. In 2003 he received his PhD in electrical engineering from Technical University of Berlin. He is an Associate Professor at Sahand University of Technology, Tabriz, Iran. His research interests are microsystem technologies, MEMS and electronic measurement systems for industrial applications.

**Esmaeil Najafi Aghdam** received MS degree in electronic engineering from Amir-Kabir University of Technology, Tehran, Iran, in 1994. In 1995, he joined the Department of Electrical Engineering at Sahand University of Technology, Tabriz, Iran, as a lecturer. In 2002, he started his PhD program dealing with a high-performance bandpass delta sigma ADC. The research program was directed by Prof. P. Benabes at SUPELEC, France. Currently, he is an Associate Professor at Sahand University of Technology. His current research interests include RF design, delta sigma converters, and electronic measurement.

**Mehmet Remzi Dokmeci** is an Associate Adjunct Professor of Radiology at the University of California-Los Angeles (UCLA). Previously, he was an Instructor of Medicine at Brigham and Women's Hospital, Harvard Medical School. He has also worked at Corning-Intellisense, a MEMS foundry and was a faculty in the Department of Electrical and Computer Engineering at Northeastern University. Dr. Dokmeci has long standing expertise in micro- and nanoscale sensors and devices and related applications to biomedical devices, organs on a chip, regenerative medicine and implantable

biosensors. He has published over 116 journal articles, 110 conference publications, 4 book chapters, and 4 patents.

**Ali Khademhosseini** is the Levi Knight Professor of Bioengineering, Chemical Engineering and Radiology at the University of California-Los Angeles (UCLA). He is the Founding Director of the Center for Minimally Invasive Therapeutics at UCLA and the Associate Director of the California NanoSystems Institute. Previously, he was a Professor of Medicine at Harvard Medical School. He is recognized as a leader in combining micro- and nano-engineering approaches with advanced biomaterials for regenerative medicine applications. He has received more than 40 awards, authored over 500 journal papers and 50 books/chapters. He is a fellow of AIMBE, BMES, RSC, FBSE, and AAAS.

**Yu Shrike Zhang** received his Ph.D. from Georgia Institute of Technology in the Wallace H. Coulter Department of Biomedical Engineering in 2013. He is currently an Instructor of Medicine and Associate Bioengineer in the Division of Engineering in Medicine at the Brigham and Women's Hospital, Harvard Medical School. Dr. Zhang's research is focused on innovating medical engineering technologies to recreate functional biomimetic tissues, including biomaterials, bioprinting, organs-on-chips, medical devices, biomedical imaging, and biosensing. He has pioneered the development of multi-sensor-integrated organs-on-chips platforms for automated, continual, and non-invasive drug screening. He is actively collaborating with a multidisciplinary team encompassing biomedical, mechanical, electrical, and computer engineers as well as biologists and clinicians to ultimately translate these cutting-edge technologies into clinics.